Environmental Science
Processes & Impacts

Controls on the photochemical production of hydrogen peroxide in Lake Erie

Journal:	*Environmental Science: Processes & Impacts*
Manuscript ID	EM-ART-08-2022-000327.R1
Article Type:	Paper

Environmental Significance Statement

Hydrogen peroxide (H_2O_2) is ubiquitous in natural waters where it influences water quality. Knowing how H_2O_2 influences water quality requires an understanding of H_2O_2 production. H_2O_2 is produced upon absorption of sunlight by organic matter in water, but too little is known about the yield of H_2O_2 from this process to predict amounts of H_2O_2 present to influence water quality. We show that the average yield of H_2O_2 in Lake Erie is within previously reported ranges for freshwaters, but there is substantial spatial and temporal variability. The yields of sunlight-produced H_2O_2 may not be high enough to influence water quality in Lake Erie (e.g., the toxicity of algal blooms).

Controls on the photochemical production of hydrogen peroxide in Lake Erie

Dhurba Raj Pandey,[1] Catherine Polik,[1] Rose M. Cory [1]†

[1]*Department of Earth and Environmental Sciences, University of Michigan*

†Corresponding Author Information: rmcory@umich.edu

Electronic Supplementary Information (ESI) available: Pandey_ESI.pdf contains supporting figures, tables and method details on the analysis of the concentration and composition of CDOM, FDOM and hydrogen peroxide.

Abstract

In Lake Erie, toxin-forming harmful algal blooms (HABs) occur following high concentrations of hydrogen peroxide (H_2O_2). Correlation between H_2O_2 concentrations and HABs revealed knowledge gaps on the controls of H_2O_2 production in Lake Erie. One way H_2O_2 is produced is upon absorption of sunlight by the chromophoric fraction of dissolved organic matter (CDOM). Rates of this photochemical production of H_2O_2 may increase in proportion to the apparent quantum yield of H_2O_2 ($\Phi_{H2O2,\lambda}$) from CDOM. However, the $\Phi_{H2O2,\lambda}$ for H_2O_2 production from CDOM remains too poorly constrained to predict the magnitude and range of photochemically produced H_2O_2, particularly in freshwaters like Lake Erie. To address this knowledge gap, the $\Phi_{H2O2,\lambda}$ was measured approximately biweekly from June – September 2019 in the western basin of Lake Erie along with supporting analyses (e.g., CDOM concentration and composition). The average $\Phi_{H2O2,\lambda}$ in Lake Erie was within previously reported ranges. However, the $\Phi_{H2O2,\lambda}$ varied 5-fold in space and time. The highest $\Phi_{H2O2,\lambda}$ was observed in the Maumee River, a tributary of Lake Erie. In nearshore waters of Lake Erie, the $\Phi_{H2O2,\lambda}$ decreased about five-fold from June through September. Integration of the controls of photochemical production of H_2O_2 in Lake Erie show that the variability in rates of photochemical H_2O_2 production was predominantly due to the $\Phi_{H2O2,\lambda}$. In offshore waters, CDOM concentration also strongly influenced photochemical H_2O_2 production. Together, the results confirm prior work suggesting that photochemical production of H_2O_2 contributes but likely cannot account for all the H_2O_2 associated with HABs in Lake Erie.

1. Introduction

H_2O_2 is a reactive oxygen species (ROS) produced in all natural waters where it is thought to cause oxidative stress and thus influence microbial community composition. [1,2]

Multiple lines of evidence suggest that high H_2O_2 concentrations in freshwaters may favor the toxin-forming strains of cyanobacterial harmful algal blooms[3] over non-toxic strains.[1,4] For instance, H_2O_2 concentrations on the high end of the range reported in freshwaters[5–7] (e.g., > 1 μM) were consistently observed in Lake Erie prior to peak toxicity of the summertime harmful algal bloom.[1,8] Assessing the potential linkage between high H_2O_2 and toxin-forming harmful algal blooms requires understanding the processes and conditions that result in high H_2O_2 concentrations in Lake Erie and similarly eutrophic waters.

H_2O_2 is produced upon absorption of ultraviolet (UV) sunlight by the chromophoric fraction of dissolved organic matter (CDOM).[9,10] Photochemical production of H_2O_2 starts with absorption of sunlight by CDOM, forming excited state CDOM*. Current understanding[11] is that photo-excited CDOM* facilitates intramolecular excited-state electron transfer processes that reduce dissolved oxygen (O_2) to superoxide (O_2^-, or its conjugate acid HO_2). Superoxide then undergoes dismutation to H_2O_2. In addition to abiotic photochemical production of H_2O_2, there is extracellular production of H_2O_2 by heterotrophic bacteria and phytoplankton (i.e., biological production).[1,12–14] Heterotrophic bacteria are the main sink for H_2O_2 in fresh and marine waters.[14,15] Prior work[1] concluded that the high H_2O_2 concentrations in Lake Erie were likely primarily due to biological production based on qualitative assessments of biological production and decay rates, abiotic photochemical production rates, and spatial and temporal patterns of H_2O_2 concentrations in the lake water.

However, one major limitation of the prior work[1] is little knowledge of the magnitude and variability of the apparent quantum yield of H_2O_2 production from CDOM ($\Phi_{H2O2,\lambda}$; defined as the mole of H_2O_2 produced per mole photon of sunlight absorbed by CDOM). Photochemical production of H_2O_2 depends strongly on the $\Phi_{H2O2,\lambda}$ [16] but little is known about how the $\Phi_{H2O2,\lambda}$ varies between waters. Literature syntheses report a fairly narrow range of $\Phi_{H2O2,\lambda}$ in coastal and

offshore seawater.[16,17] Thus, Cory *et al*. (2016) used an average $\Phi_{H2O2,\lambda}$ reported from measurements in coastal and offshore seawater[16,17] to estimate photochemical production of H_2O_2 in Lake Erie. However, some evidence suggests that $\Phi_{H2O2,\lambda}$ depends on dissolved organic matter (DOM) composition, such that the $\Phi_{H2O2,\lambda}$ increases with increasing proportion of terrestrially-derived DOM.[17,18] For example, higher $\Phi_{H2O2,\lambda}$ have been reported in freshwater than seawater, consistent with the greater proportion of terrestrially-derived DOM in freshwater than in seawater DOM.[17,18] Of the few measurements of the $\Phi_{H2O2,\lambda}$ in freshwaters, none come from eutrophic freshwaters like Lake Erie where the source and composition of DOM shifts substantially from relatively more terrestrially-derived DOM exported via rivers during spring storms to autochthonously-derived DOM over the course of the summertime algal bloom.[1] Thus, if the $\Phi_{H2O2,\lambda}$ is higher or spans a more dynamic in range in Lake Erie than in seawater, photochemical production may account for a larger or more variable share of H_2O_2 than previously estimated.[1]

Beyond Lake Erie, constraining photochemical production of H_2O_2 by CDOM is important in light of increasing CDOM concentrations over the past 30 years in North American and European freshwaters.[19–21] Increasing concentrations of terrestrially-derived CDOM in freshwaters is expected to result in greater photochemical production of H_2O_2.[22] In turn, toxin-forming HABs have been predicted to increase with increasing CDOM (and H_2O_2) concentrations.[23] However, predicting the extent to which increasing CDOM may result in higher photochemical production of H_2O_2 requires knowledge of how the $\Phi_{H2O2,\lambda}$ interacts with the two other major controls on photochemical production of H_2O_2: CDOM concentration and the UV photon flux.[1] In relatively low CDOM waters, rates of photochemical processes increase with increasing CDOM. For example, in low CDOM waters, photochemical H_2O_2 production may be limited by CDOM concentration (substrate limited by concentration). Once

the CDOM concentration is sufficiently high enough to absorb all photons reaching the water surface, photochemical H_2O_2 production reaches an asymptote where increasing CDOM no longer increases H_2O_2 production. Under the latter conditions, rates of photochemical processes are characterized as sunlight-limited.[24] In addition to limitations by CDOM concentration and sunlight, the $\Phi_{H2O2,\lambda}$ of CDOM may be the predominant limit on photochemical H_2O_2 production (i.e., substrate limitation by the composition of CDOM that may control yields of H_2O_2). In any water, it is the interaction between these three controls ($\Phi_{H2O2,\lambda}$, CDOM concentration, and photon fluxes), along with water column depth, that determines whether a photochemical process is substrate (concentration or composition) or sunlight-limited.

Investigating these limitations over the ranges of $\Phi_{H2O2,\lambda}$, CDOM concentration, and photon fluxes is critical in freshwaters to understand how changes in CDOM concentration[20,25] may affect photochemical production of H_2O_2, and in turn, may influence HABs. Thus, the objectives of this study were: 1) to quantify the magnitude and variability of the apparent quantum yield of H_2O_2 production from CDOM ($\Phi_{H2O2,\lambda}$) in Lake Erie, and 2) to quantify the influences of $\Phi_{H2O2,\lambda}$, CDOM concentration, and photon fluxes on photochemical production of H_2O_2 in Lake Erie based on the ranges of these controls over the summer in Lake Erie.

2. Methods

2.1 Site description and sampling

Water samples were collected from the Maumee River, one of the largest contributors of nitrogen and phosphorous to the western basin of Lake Erie.[26] Given the importance of the Maumee River nutrient load to the western basin of Lake Erie, it is likely that the Maumee River is also an important source of terrestrially-derived DOM (and thus CDOM) to the western basin of Lake Erie. The Maumee River was sampled at Waterworks Park (41º 29' 37" N, 83º 42' 58" W; Waterville, OH) approximately once a month from June through September 2019. The water

samples were collected from slightly below the water surface of the river by dipping a 2 L amber high-density polyethylene (HDPE) bottle into the river. The water samples were stored in the dark on ice during transport (< 2 hour) back to the laboratory at the University of Michigan.

Lake Erie was sampled weekly from late May through early October 2019 from two of the National Oceanic and Atmospheric Administration (NOAA) monitoring sites in the western basin of Lake Erie: sites WE2 and WE4.[1,27] The physical and biogeochemical characteristics of waters at WE2 and WE4 have been described extensively in prior studies.[1,27,28] Briefly, WE2 is approximately 15 km from the mouth of the Maumee River, and site WE4 is about another 15 km farther offshore compared to WE2. Being closer to the Maumee River than WE4, site WE2 has higher specific conductivity, higher CDOM concentrations[1] and is more affected by the harmful algal blooms (HABs) than WE4.[27] Depth integrated water samples were collected at each site, with the depth ranging from 0-5 m at WE2 and 0-8 m at WE4. Water was collected in a 2 L HDPE bottle and stored in the dark on ice during transport (2-6 hours) back to the laboratory at the University of Michigan. Weekly sampling at WE2 and WE4 from May through October 2019 resulted in collection of water samples before, during, and after a harmful algal bloom in the western basin of Lake Erie.[29] Several water samples were also collected from the western basin of Lake Erie on dates and locations associated with high bloom activity during (July and August, 2019) and after (September, 2019) the harmful algal bloom (collectively called high bloom biomass water samples). The sampling locations for high bloom biomass water samples in July and August were areas in the western basin of Lake Erie showing maximum algal growth in the weekly HABs forecast.[29] All high bloom biomass sites were closer to the shore in the western basin than is WE2.

Upon arrival in the laboratory, all water samples were immediately filtered through a 0.22 μm polyethersulfone (PES) filter. Subsamples of the filtered water for analysis of the

concentration of dissolved organic matter (i.e., dissolved organic carbon, DOC) were preserved by addition of 6N trace metal grade hydrochloric acid to pH 3 and stored in 120 mL amber HDPE bottles. Subsamples of filtered water for analysis of CDOM and the fluorescent fraction of dissolved organic matter (FDOM) were stored in 30 mL amber HDPE bottles. Subsamples of filtered water for the apparent quantum yield spectrum measurements ($\Phi_{H2O2,\lambda}$) were stored in 2 L amber HDPE bottles. All subsamples were stored in the dark at 4 ^{o}C until analysis.

2.2 Analysis of DOC, CDOM, and FDOM

Water samples were analyzed for DOC concentration on a Shimazdu TOC-V analyzer (CV~3% on duplicate analyses[30]). Absorption coefficients of CDOM and optical proxies for CDOM composition were analyzed on an Aqualog Spectrofluorometer (Horiba Scientific) in a 1 cm pathlength quartz cuvettes as previously described.[1] The spectral slope ratio (S_R) of CDOM, a proxy for the average molecular weight of DOM, was calculated from the absorbance spectrum for each water sample.[31] Naperian absorption coefficients of CDOM ($a_{CDOM\lambda}$, m^{-1}) were calculated from the CDOM absorbance spectrum as:

$$aCDOM_\lambda = \frac{A_\lambda}{L} 2.303 \qquad Eq.1$$

Where A is the decadic absorbance reading and L is the pathlength of the quartz cuvette (m). The specific UV absorbance at 254 nm ($SUVA_{254}$; L mg^{-1} C m^{-1}), a proxy for the average aromatic carbon content of the DOM, was calculated by dividing absorbance at 254 nm (A_{254}) by the cuvette pathlength (m) and DOC concentration (mg C L^{-1}).[32]

FDOM was measured as an excitation emission matrix (EEM) spectrum on the Aqualog Spectrofluorometer (Horiba Scientific) in a 1 cm pathlength quartz cuvettes as previously described.[1] From the EEM spectra, proxies for FDOM composition were calculated as ratios of the dominant peaks A, C, and T.[1] The fluorescence Index (FI), a proxy for relative contributions

of terrestrially-derived (allochthonous) and autochthonously-derived CDOM was calculated following Cory et al. 2016. The attribution of CDOM sources to the FDOM peak ratios and their distributions in the western basin of Lake Erie have been described in detail in Cory et al. 2016. Briefly, the FDOM peaks A and C are associated with terrestrially-derived CDOM from the breakdown products of lignin.[33] Peak T is associated with aromatic amino acids, and often relatively higher intensities of peak T are observed in waters with relatively more autochthonously-derived DOM than terrestrially-derived DOM.[33] Thus, the ratio of FDOM intensities at peak T to peak A (T/A ratio) provides a qualitative assessment of the abundance of amino acid-like FDOM (associated with autochthonous DOM) relative to terrestrially-derived DOM.[33] Differences in water chemistry between sites were determined to be statistically significant if the difference in the average was greater than 1 standard error of the average at each site.

2.3 Apparent quantum yield spectra

The apparent quantum yield spectrum of H_2O_2 production from CDOM ($\Phi_{H2O2,\lambda}$) was quantified from filtered water samples within 7-9 days of sampling. Water samples were warmed to room temperature for ~ 5 hours before separation into light-exposure and dark control treatments. A subset of each water sample was prepared for the light-exposure treatment by placing water in triplicate gas-tight, flat-bottomed 12 mL quartz vials. A subset of each water sample was prepared for the dark control by placing water in triplicate gas-tight, borosilicate tubes wrapped in aluminum foil. The diameter (12 mm), length and thus volume of the quartz tubes used for the light-exposure treatment was the same as the borosilicate tubes used for the dark controls.

Light treatment samples were exposed to simulated sunlight in a Suntest XLS solar simulator (Atlas Materials) equipped with a 1.5 kW Xenon lamp as the light source set to 750 W

m^{-2}. Subsamples were collected every 20 minutes for H_2O_2 concentration from both the light-exposure and dark control treatments, beginning with the start of the experiment (0 minutes) to up to 120 minutes of light exposure. Water temperature was measured from one replicate of each light-exposure and dark control treatments at the end of each experiment. Water temperature was 29 ± 0.1 °C in the light-exposure treatments and 23 ± 0.1 °C in the dark control treatments (n = 41 temperature measurements from each light-exposure and dark control treatments). Following light-exposure, all water samples were wrapped in aluminum foil and stored at 4 °C overnight prior to measuring H_2O_2 concentrations.

H_2O_2 concentration in the light-exposure and the dark control treatments were measured within 24 hours of the experiment using the Amplex® Red assay (Invitrogen Co.).[1,8] H_2O_2 concentration was measured as the production of resorfurin on an ultra-Performance Liquid Chromatograph (uPLC, Waters Technology) at an excitation wavelength of 565 nm and emission wavelength of 587 nm using an Acquity uPLC BEH C_{18} column (2.1 mm x 50 mm x 1.7 μm).[1] H_2O_2 concentration was quantified by standard addition to minimize potential sample matrix effects.[1] There was no evidence of decay of H_2O_2 during overnight storage in the dark prior to analysis (Figure S1). No detectable decay of H_2O_2 in filtered water in the dark is consistent with biological decomposition as the predominant sink of H_2O_2,[14,15] particularly in waters like Lake Erie with low concentrations of trace metals such as copper or iron that are abiotic sinks for H_2O_2.[34]

H_2O_2 concentrations were plotted versus experiment time to quantify an experimental production rate for both light-exposure and dark control treatments. Production rates were fit linearly using least-squares regressions. T-tests were used to determine whether the slope of each linear regression was significantly different from zero, with statistical significance was defined as $p < 0.05$. A production rate of H_2O_2 was quantified when the slope of H_2O_2

concentration vs. experiment time was significantly different than zero for both light-exposure and dark control treatments. There was significant H_2O_2 production in the light-exposure treatment for 40 out of 41 water samples. Significant H_2O_2 production in dark control treatments was observed in 35 out of 41 water samples as an artifact of the Amplex® Red method (see electronic supplementary information). Significant dark H_2O_2 production was subtracted from the respective H_2O_2 production rate in the light-exposed treatment to obtain an experimental light minus dark rate of H_2O_2 production ($P_{H2O2,exp}$). $P_{H2O2,exp}$ was significantly different than zero in 39 out of 41 water samples. The standard error (SE) of $P_{H2O2,\,exp}$ was calculated as the square root of the sum of the squared standard error of each of the dark control and light-exposed slope of H_2O_2 concentration vs. experiment time.

The $P_{H2O2,exp}$ (mol $m^{-3}s^{-1}$) is the product of the $\Phi_{H2O2,\lambda}$ (mol H_2O_2 mol^{-1} photons) and the rate of photon absorption by CDOM ($Q_{a,\lambda}$; mol photons m^{-2} s^{-1}):

$$P_{H2O2,\,exp} = \int_{\lambda_{min}}^{\lambda_{max}} \phi_{H2O2,\lambda}\ Q_{a,\lambda} \qquad Eq.2$$

Where λ_{min} and λ_{max} are the maximum and minimum wavelength of the simulated light (280 and 600 nm respectively). $Q_{a,\lambda}$ is calculated as:

$$Q_{a,\lambda} = \int_{\lambda_{min}}^{\lambda_{max}} \left(1 - e^{-aCDOM_{\lambda}L}\right) E_{0\lambda} \qquad Eq.3$$

Where L is the pathlength of the quartz tubes (12 mm). The total light absorbed ($Q_{a,280\text{-}600}$) by CDOM during the experiments to quantify $\Phi_{H2O2,\lambda}$ ranged from 0.3 µmol photons m^{-2} in the lowest CDOM water (site WE4 in Lake Erie) to 30 µmol photons m^{-2} in the highest CDOM water (Maumee River). The photon flux spectrum ($E_{0,\lambda}$; mol photons m^{-2} s^{-1}) reaching the quartz tubes was measured at 1 nm intervals with a UV-Visible portable radiometer[35] (Ocean Optics, USA). The $\Phi_{H2O2,\lambda}$ is the unknown in *Eq.2* and is solved for by assuming that it is a spectrum that decreases exponentially with increasing wavelength:[36]

$$\Phi_{H2O2,\lambda} = c\, e^{(-d\,\lambda)} \quad Eq.4$$

Where c (mol H_2O_2 mol^{-1} photons) and d (nm^{-1}) are positive parameters and λ is the wavelength. The $\Phi_{H2O2,\lambda}$ of each water sample was calculated using an unconstrained nonlinear optimization (fminsearch function in Matlab R2018a) such that c and d gave the best fit between measured and calculated H_2O_2 production rates (minimum relative error between measured and calculated photo production rates, with initial guesses of 1 and 0.03 for c and d parameters, respectively). Uncertainty in each $\Phi_{H2O2,\lambda}$ was determined by solving *Eq.4* for $P_{H2O2,exp}$ ± 1 SE. To compare the magnitude of the $\Phi_{H2O2,\lambda}$ between different water samples in this study and in the literature, the apparent quantum yield at 350 nm ($\Phi_{H2O2,350}$) was reported as the average ± 1 SE of the experimental replicates (n=3).

The magnitude and shape of the $\Phi_{H2O2,\lambda}$ spectrum was tested on two water samples using a new, custom-built high-powered (≥ 100 mW), narrow-banded (± 10 nm) light-emitting diode (LED) system developed for measurement of apparent quantum yield spectra.[35,37] Briefly, water from the Maumee River and Lake Erie site WE2 was collected on 6-July-21 and 14-July-21, respectively, and filtered and equilibrated to room temperature as described above. Water was placed in duplicate in the same gas-tight, flat-bottomed 12 mL quartz vials (light treatment) and 12 mL borosilicate exetainer vials (dark controls) as used for the solar simulator experiments described above. Vials were placed in an inner black plastic housing (to minimize light scattering), with the flat bottom facing upward toward the light source, and then exposed to ≥ 100 mW, narrow-banded (± 10 nm) LEDs at 275, 365, 385, and 405 nm alongside the dark controls for the period of time sufficient for the CDOM to absorb 0.05 mol photons m^{-2} at each wavelength (from 58 to 152 minutes depending on the wavelength of LED light). Immediately after LED exposure, light-exposed and dark control waters were analyzed for H_2O_2 by the

Felume method.[1,8,38]

Prior to light exposure, dissolved oxygen concentrations in the water samples were near saturation (~ 280 μM). Zhang et al. (2012)[39] reported that photochemical production of H_2O_2 may be limited by O_2 at concentrations below 300 μM dissolved O_2. However, H_2O_2 production increased linearly with increasing light exposure over the duration of the experiment (Figure S2). Thus, O_2 limitation on $\Phi_{H2O2,\lambda}$ was not detected in these experiments.

2.4 Photochemical production rates of H_2O_2 in Lake Erie

The photochemical production rate of H_2O_2 by CDOM in the water column of Lake Erie ($P_{H2O2,\ lake}$; mmol H_2O_2 m^{-2} day^{-1}) was calculated using the $\Phi_{H2O2,\lambda}$ (mmol H_2O_2 mol^{-1} photons) and the rate of light absorption by CDOM in Lake Erie ($Q_{a,\lambda}$; mol photons m^{-2} day^{-1}):

$$P_{H2O2,lake} = \int_{\lambda_{min}}^{\lambda_{max}} \phi_{H2O2,\lambda}\, Q_{a,\lambda}\, \frac{aCDOM_\lambda}{atot_\lambda}\, d\lambda \qquad Eq.5$$

Where λ_{min} and λ_{max} are the range of UV and visible sunlight (from 280 to 600 nm, respectively), $a_{CDOM,\lambda}/a_{tot,\lambda}$ is the fraction of light absorbed by CDOM compared to light absorbed by all constituents in the water (CDOM, particles and water; $a_{tot,\lambda}$). Prior work reported that $a_{CDOM,\lambda}/a_{tot,\lambda}$ ranged from 0.72 ± 0.02 at 305 nm to 0.67 ± 0.02 at 412 nm in Lake Erie (average ± 1 SE, n =64).[1] Because the goal of this study is to calculate the maximum possible photochemical H_2O_2 production in Lake Erie, a ratio of $a_{CDOM,\lambda}/a_{tot,\lambda} = 1$ was used at all wavelengths. $Q_{a,\lambda}$ is the light absorbed by CDOM in the water column (*Eq.3)*. In *Eq. 5*, $Q_{a,\lambda}$ was calculated over a water column depth of 1 m in Lake Erie because on average 99% of UV light was absorbed by CDOM within 1 m in Lake Erie.[1] A daily photon flux spectrum reaching the western basin of Lake Erie corresponding to the day of sample collection during summer 2019 was obtained by integrating the hourly photon flux for 12 hours (7AM-7PM Eastern Standard Time) over 280-600 nm (1 nm increments). Hourly photon fluxes were obtained from spectral

direct and diffuse irradiances reaching the surface of Lake Erie from the Tropospheric Ultraviolet and Visible (TUV) radiation model (version 5.3).[40] The model was run with a four-stream discrete ordinate radiative transfer method with a pseudo-spherical modification. The model used an overhead ozone column of 300 Dobson units, a surface albedo of 10%, and cloud free skies.

To investigate the sensitivity of photochemical H_2O_2 production to the amount of sunlight (photon flux, $E_{0,\lambda}$), CDOM, or $\Phi_{H2O2,\lambda}$, each term was varied independently in *Eq. 5*, using the average, minimum, and maximum values observed at sites WE2 and WE4 in Lake Erie. Maximum, average and minimum photon fluxes were obtained from the period of May 21 through October 7 2019 as described above. Maximum, average and minimum CDOM were obtained from a dataset of summertime CDOM concentrations collected from 2014-2020 at WE2 and WE4 (e.g., from Cory et al. 2016 and this study). Maximum, average and minimum $\Phi_{H2O2,\lambda}$ are from this study at WE2 or WE4.

2.5 Temperature correction of apparent quantum yield spectra

The apparent quantum yield spectra were quantified in the laboratory ($\Phi_{H2O2,\lambda,Texp}$) from water samples having an average water temperature of 29 ± 0.1 °C (n = 41). Given that the $\Phi_{H2O2,\lambda}$ have been reported to depend on water temperature,[16] the $\Phi_{H2O2,\lambda,Texp}$ were converted to the lake surface water temperature ($\Phi_{H2O2,\lambda,Tlake}$) at each site on the date of sample collection:[16]

$$ln\frac{\Phi_{H2O2,\lambda,Tlake}}{\Phi_{H2O2,\lambda,Texp}} = \frac{E_a}{R}\left(\frac{1}{T_{exp}} - \frac{1}{T_{lake}}\right) \quad Eq.6$$

Where T_{exp} is the experimental water temperature and T_{lake} is the Lake Erie water temperature, R is the universal gas constant and E_a is the activation energy. A constant E_a of 21.8 KJ mol^{-1} was used for all wavelengths (280-600 nm).[16]

3. Results and discussion

3.1 Spatial and temporal patterns in water and dissolved organic carbon chemistry

The range in water temperature and water chemistry values overlapped with prior work in the western basin of Lake Erie during the summer.[1] Thus, trends in DOM concentration and composition reported in this study are representative of summertime ranges in the western basin of Lake Erie. There were no significant differences in average water temperature or pH between the Maumee River and Lake Erie (Table 1). Trends in water chemistry shifted along the riverine to offshore site in Lake Erie, consistent with prior work in this basin.[1] For example, specific conductivity, DOC concentration, and CDOM absorption coefficients at 305 nm (a_{305}) were highest in the Maumee River, followed by site WE2 in Lake Erie (the site closer to the Maumee River), and lowest at the relatively offshore site WE4 (Table 1). Likewise, CDOM and FDOM composition shifted from relatively more to less terrestrially-derived DOM from the riverine to offshore site. For example, S_R increased and $SUVA_{254}$ decreased from the Maumee River to WE2 to WE4, indicating higher average molecular weight[31] and aromatic carbon content[32] of the DOM, respectively, from the river to offshore Lake Erie (Table 1). FDOM in the Maumee River had a lower FI and T/A ratio, indicating greater aromatic carbon content and relatively less amino acid-like FDOM, respectively, compared to FDOM in Lake Erie (Table 1). FDOM at WE2 had a lower T/A ratio compared to WE4 (Table 1).

DOC concentration was higher in high bloom biomass waters than at WE2 and WE4 (Table 1). a_{305} was not significantly different between high bloom biomass waters and WE2 (Table 1). CDOM and FDOM proxies for DOM composition showed that high bloom biomass waters had similar DOM composition to the DOM at site WE2. For example, S_R, $SUVA_{254}$, and FDOM T/A of high bloom biomass waters were not significantly different compared to WE2 (Table 1).

DOC concentration and a_{305} generally decreased from May through October in the Maumee River and at site WE2 in Lake Erie (shown for a_{305} at WE2 in Figure 4). The composition of CDOM and FDOM shifted from May through October, in the Maumee River and at site WE2, from relatively more to less terrestrially-derived DOM as indicated by the decrease in $SUVA_{254}$ (Figure S3) and an increase in the FI and T/A ratio (Figure S4, Figure S5). At WE4, the FI generally increased from May through October (Figure S4). There was no clear temporal pattern in other CDOM or FDOM proxies for DOM composition at WE4 from May through October (Figure S3 and S5).

3.2 Spatial and temporal patterns in the H_2O_2 apparent quantum yield

The experimental (laboratory) rate of H_2O_2 production ($P_{H2O2,exp}$) increased significantly with increasing CDOM concentration (a_{305}; Figure 1, $p < 0.0001$). Increasing production of H_2O_2 with increasing CDOM is expected in filtered water exposed to light, i.e., when abiotic photochemical production of H_2O_2 by CDOM is the only source of the H_2O_2 in the water (*Eq.2*). Given similar light exposure times and photon fluxes during the experiments to quantify $P_{H2O2,exp}$, a significant deviation from the linear regression of $P_{H2O2,exp}$ vs. a_{305} suggests a difference in the apparent quantum yield of H_2O_2 ($\Phi_{H2O2,\lambda}$) from CDOM relative to all water samples in the dataset (Figure 1). For example, three of four Maumee River waters and several WE2 waters had significantly higher H_2O_2 production than predicted from the linear regression of $P_{H2O2,exp}$ vs. a_{305} (Figure 1). Thus, these results justify quantification of the $\Phi_{H2O2,350}$ (*Eq. 4*) for each water sample.

Overall, the average and range of the magnitude of the $\Phi_{H2O2,\lambda}$ in the Maumee River and Lake Erie are within the range previously reported for freshwaters[6,10,18,36] and higher than the average reported for seawater (Figure S10).[16,17] The average $\Phi_{H2O2,350}$ in the Maumee River water was significantly higher than the average $\Phi_{H2O2,350}$ at each site in Lake Erie (Figure 2).

On average, there was no significant difference in the $\Phi_{H2O2,350}$ between the nearshore site WE2 and offshore site WE4 (Figure 2). Likewise, there was no significant difference in the average $\Phi_{H2O2,350}$ of the high bloom biomass waters and the average $\Phi_{H2O2,350}$ of WE2 and WE4 waters (Figure 2). The $\Phi_{H2O2,350}$ decreased approximately five-fold at WE2 in Lake Erie from 0.52 ± 0.04 mmol H_2O_2 mol^{-1} photons in early June to 0.11 ± 0.10 mmol H_2O_2 mol^{-1} photons in early October (Figure 3). No clear temporal trend in the $\Phi_{H2O2,350}$ was observed in high bloom biomass and WE4 waters (Figure S9). There were no significant correlations between the $\Phi_{H2O2,350}$ and any optical proxies of CDOM or FDOM composition (e.g., S_R, FI, or ratios of FDOM peaks; data not shown). However, the $\Phi_{H2O2,350}$ averaged by site was significantly, positively correlated with the site- averaged $SUVA_{254}$ ($p < 0.05$; Figure S6).

The $\Phi_{H2O2,350}$ corrected to Lake Erie water temperature generally was not significantly different than the experimentally determined $\Phi_{H2O2,350}$ (shown for WE2 in Figure S6). A small effect of temperature on the $\Phi_{H2O2,350}$ was expected due to generally small differences between experimental and lake water temperature (Figure S7). The exceptions were a few waters collected in May or June when Lake Erie water temperatures were approximately 10 °C less than the average water temperature during the experiments to quantify the $\Phi_{H2O2,\lambda}$. For these waters, the $\Phi_{H2O2,350}$ was on average 27% lower than the experimentally quantified $\Phi_{H2O2,350}$ (Figure S6). Thus, because temperature correction did not significantly impact spatial or temporal patterns of the $\Phi_{H2O2,350}$ in Lake Erie, daily photochemical production rates in Lake Erie were calculated using the uncorrected, experimental $\Phi_{H2O2,\lambda}$ at each site.

Photochemical H_2O_2 production as a function of LED wavelength confirmed that an exponentially decreasing $\Phi_{H2O2,\lambda}$ with increasing wavelength was the best fit for the $\Phi_{H2O2,\lambda}$ spectrum (Figure S11). This result is expected based on other studies that have directly quantified the wavelength dependence of $\Phi_{H2O2,\lambda}$ in natural waters.[36,41] The reason for the

decrease in $\Phi_{H2O2,\lambda}$ with increasing wavelength is not known. Others have speculated that these results may be due to a relationship between size and reactivity of fractions of CDOM. For example,[42] speculated that light of longer wavelengths is preferentially absorbed by larger CDOM fractions that are less reactive than smaller CDOM moieties.

The LED results show that the $\Phi_{H2O2,\lambda}$ spectrum of Maumee River was significantly higher (at all wavelengths) than site WE2 in Lake Erie (Figure S11). Thus, the LED result for the $\Phi_{H2O2,\lambda}$ agreed with the solar simulator results of the larger dataset showing that on average, the $\Phi_{H2O2,350}$ of the Maumee River is greater than that of WE2 in Lake Erie (Figure 2).

3.3 Terrestrially-derived DOM may control the magnitude of the H_2O_2 apparent quantum yield

Three lines of evidence support that terrestrially-derived DOM is a control on the magnitude of the $\Phi_{H2O2,\lambda}$. First, the average $\Phi_{H2O2,350}$ in the Maumee River was higher than the average $\Phi_{H2O2,350}$ of the Lake Erie waters (Figure 2). This result is consistent with the higher proportion of terrestrially-derived DOM in the Maumee River than in Lake Erie (Table 1, Figure S1), and with the positive correlation between the average $\Phi_{H2O2,350}$ and the average $SUVA_{254}$ (by site, Figure S8).

Second, the $\Phi_{H2O2,350}$ decreased from June through October at site WE2 (Figure 3). A decrease in the $\Phi_{H2O2,350}$ at WE2 over the summer is consistent with decreasing inputs of terrestrially-derived DOM from the Maumee River to Lake Erie over this time period (Figure S1). For example, a decrease in the aromatic content of DOM at WE2 ($SUVA_{254}$; Figure S3), a proxy for the proportion of terrestrially-derived DOM, suggests decreasing terrestrially-derived DOM to nearshore waters like WE2 from June through October. Previous work also reported decreasing inputs of terrestrially-derived DOM to nearshore waters of Lake Erie over the summer.[1] Lower export of terrestrially-derived DOM to nearshore waters of Lake Erie over the

summer is consistent with decreasing discharge from the Maumee River over the summer.[43]

Third, autochthonously-derived DOM can produce H_2O_2 photochemically,[44] thus its influence may be to lower the magnitude of the $\Phi_{H2O2,\lambda}$ compared to that of terrestrially-derived DOM. For example, DOM from autochthonous sources (e.g., bacterial and algal matter present in the high bloom biomass water) in high bloom waters was not significantly different than at sites WE2 and WE4 (Figure 2). Likewise, the high bloom biomass water had a DOM composition that overlapped with the DOM composition at WE2 and WE4 (Table 1, Figures S3-S5), consistent with the greater contributions of autochthonous carbon to the DOM pool in Lake Erie (compared to the river). Alternatively, it may be that the magnitude of the $\Phi_{H2O2,\lambda}$ is controlled predominantly by the proportion of terrestrially-derived DOM, such that loss (e.g., degradation or dilution) of terrestrially-derived CDOM in the nearshore, offshore or high bloom biomass water relative to the river caused the decrease in the $\Phi_{H2O2,350}$ compared to the Maumee River. This interpretation is consistent with prior work showing no difference in the $\Phi_{H2O2,\lambda}$ upon dilution of river water with coastal water,[36] where the coastal water was inferred to contain a greater proportion of autochthonous DOM compared to the river water. The influence of terrestrially-derived DOM on the $\Phi_{H2O2,350}$ in Lake Erie is consistent with prior work in other waters.[45] For example, O'Sullivan et al (2005)[18] suggested that the higher magnitude of $\Phi_{H2O2,\lambda}$ in river waters compared to the coastal waters was due to relatively more terrestrially-derived DOM in the river than in the coastal water. Powers and Miller (2014)[17] also suggested the higher magnitude of $\Phi_{H2O2,\lambda}$ in freshwaters compared to the coastal and open seawater may be due to the high proportion of terrestrially-derived DOM in freshwaters.

3.4 Temporal patterns in photochemical production rates of H_2O_2 in Lake Erie

Photochemical production rates of H_2O_2 at site WE2 in Lake Erie ($P_{H2O2,lake}$) decreased approximately 10-fold at WE2 from 2.6 ± 0.2 mmol H_2O_2 m^{-2} day^{-1} in early June, 2019 to 0.3 ±

0.2 mmol H_2O_2 m^{-2} day^{-1} in early October, 2019 (Figure 3). This seasonal pattern in $P_{H2O2,lake}$ at WE2 is due to peak CDOM concentration, photon flux, and the ΦH2O2,λ in June and early July compared to August through October (Figure 3). In contrast to WE2, no clear seasonal pattern was observed in $P_{H2O2,lake}$ at WE4 during summer 2019 (Figure S9). However, there was approximately a 3-fold difference between the highest $P_{H2O2,lake}$ of 1.4 ± 0.4 mmol H_2O_2 m^{-2} day^{-1} in early July and the lowest $P_{H2O2,lake}$ of 0.5 ± 0.3 mmol H_2O_2 m^{-2} day^{-1} in late July (Figure S9).

3.5 CDOM and sunlight controls on photochemical production of H_2O_2 in Lake Erie

Quantification of the dependence of $P_{H2O2,lake}$ on the photon flux, CDOM and $\Phi_{H2O2,\lambda}$ over their respective ranges at sites WE2 and WE4 (Figure 4) shows the sensitivity of $P_{H2O2,lake}$ to these controls. For example, holding the photon flux and $\Phi_{H2O2,\lambda}$ constant at the average observed in this study during summer 2019 and varying CDOM (e.g., a_{305}) between its minimum to average concentration observed during the summer at WE2 from this study and prior work (Table S1),[1] rates of H_2O_2 photochemical production increase (Figure 4). That is, a 6-fold difference between the minimum and average CDOM concentration at WE2 results in a 3-fold increase in $P_{H2O2,lake}$ (Figure 4). In contrast, a 4-fold difference between the average and maximum CDOM concentration results in little (~ 1.1-fold) increase in $P_{H2O2,lake}$ (Figure 4). This result is because $P_{H2O2,lake}$ reaches an asymptote at an a_{305} of 6 m^{-1} (in the top 1 m of the water column; *Eqs. 2-3*). The average a_{305} at WE2 is significantly higher than 6 m^{-1} (9 ± 1 m^{-1}, average ± 95% confidence interval; Table S1). Thus, at WE2 on average there is enough CDOM in the surface water to absorb all the available photon flux such that increasing the CDOM concentration above the average has a minimal impact on photochemical H_2O_2 production rates (Figure 4). Holding the photon flux and CDOM constant at their respective averages at WE2 shows that the 5-fold difference between the minimum and maximum $\Phi_{H2O2,\lambda}$ at WE2 (Figure 3, Table S1) results in a 5-fold difference between the minimum and maximum of $P_{H2O2,lake}$ (Figure

4). This result is due to the linear dependence of $P_{H2O2,lake}$ on the magnitude of the $\Phi_{H2O2,\lambda}$ (*Eq.3*). Finally, holding the CDOM and $\Phi_{H2O2,\lambda}$ constant and varying the photon flux between its minimum, average and maximum shows that a 2-fold increase from the minimum and maximum results in a 2-fold increase in $P_{H2O2,lake}$ (Figure 4). For instance, at the end of the summer when the photon flux is decreasing (and less than the average; Figure 3), CDOM can absorb more sunlight than is available (Figure 4).

At WE4, the average a_{305} is significantly lower than the CDOM concentration where $P_{H2O2,lake}$ asymptotes (3 ± 1 m^{-1} vs. 6 m^{-1}, respectively, Table S1). At WE4 on average there is not enough CDOM in the surface water to absorb the available photon flux. Thus, photochemical H_2O_2 production rates increase nearly in proportion to increasing CDOM concentration at WE4 (Figure 4). Like at WE2, the $P_{H2O2,lake}$ increases linearly with increasing $\Phi_{H2O2,\lambda}$ (*Eq.3*; Figure 4). The same photon flux was used for WE2 and WE4. Thus, the impact of varying the photon flux between its average, maximum and minimum was the same at WE4 as at WE2 (Figure 4, Table S1).

$P_{H2O2,lake}$ at both WE2 and WE4 is most sensitive to variability in the $\Phi_{H2O2,\lambda}$ over the observed ranges of the three spectra that influence $P_{H2O2,lake}$ (CDOM, $\Phi_{H2O2,\lambda}$ and photon flux; Figure 4). Therefore, in these waters, variability in photochemical H_2O_2 production rates is driven mainly by CDOM composition (substrate-limited by composition). At WE4, photochemical H_2O_2 production rates are also limited by CDOM concentration (substrate-limited by concentration). At both WE2 and WE4, photochemical H_2O_2 production rates may also limited by sunlight, such as at the end of the summer when photon fluxes are less than the summer average.

These results were generated with the assumption that CDOM is the main UV light-absorbing constituent in the water column ($a_{CDOM,\lambda}/ a_{Tot,\lambda} = 1$; *Eq. 5*). In the western basin of

Lake Erie, CDOM accounts for 60–70% of UV absorbance in the water column on average.[1] The fraction of UV light absorbed by CDOM was approximately 1 at offshore stations including WE4.[1] The fraction of UV light absorbed by CDOM was lower than the average of 60-70% at WE2 and other nearshore stations during high bloom activity or after storms when turbidity was high.[1] Thus, at nearshore sites like WE2, photochemical H_2O_2 production may also be limited by competition between CDOM and particles to absorb UV light. Alternatively, light-absorbing particulate matter may undergo photo-dissolution to produce CDOM,[46] which in turn may produce H_2O_2.

Dissolved oxygen may be a minor limitation on photochemical H_2O_2 production in the surface waters of Lake Erie. The surface waters in the western basin of Lake Erie are oxic,[47] with a summertime average dissolved oxygen in the upper 0.75 m of water in western Lake Erie during this study of 222 ± 4 μM (average ± 1 SE;[48]). This concentration of dissolved oxygen is within the range previously reported to limit photochemical production of H_2O_2.[39] However, the latter in-situ measurements of dissolved oxygen are likely lower than the upper 0.1 to 0.5 m of the water column where most photochemical H_2O_2 is made.[1] For example, the high rates of photosynthesis during the summer in the water column of Lake Erie,[27] contribute O_2 to the surface water.

4. Conclusions and implications

The magnitude of the apparent quantum yield of H_2O_2 ($\Phi_{H2O2,\lambda}$) from CDOM varied by at least five-fold in the western basin of Lake Erie, a eutrophic freshwater. The magnitude of the $\Phi_{H2O2,\lambda}$ likely depends on the proportion of terrestrially-derived DOM, and may not be influenced from DOM derived from bloom biomass. In Lake Erie, the main driver of the variability in photochemical H_2O_2 production rates is $\Phi_{H2O2,\lambda}$ (i.e., limitation by CDOM composition). Photochemical H_2O_2 production rates are also limited by sunlight in Lake Erie,

particularly when photon fluxes are lower than summer averages such as on cloudy days or towards the end of the summer season. In offshore waters, photochemical H_2O_2 production rates are also limited by CDOM concentration. These results have implications for the effects of increasing CDOM concentrations in North American and European freshwaters.[19,20]

One expectation is that as CDOM concentrations increase, so will H_2O_2 concentrations, which in turn may influence the toxicity of HABs.[1,23,49] However, results from this study show that the effects of increasing CDOM concentration on photochemical H_2O_2 production likely depends more strongly on the $\Phi_{H2O2,\lambda}$ of the CDOM than on CDOM concentration in waters like nearshore waters of Lake Erie. This is because in freshwaters rich in terrestrially-derived CDOM, such as the nearshore waters of Lake Erie, CDOM concentrations may be on average sufficiently high enough to absorb the available photon flux. In waters with sufficiently high CDOM, photochemical H_2O_2 production rates are not as sensitive to increasing CDOM as to the composition of the CDOM ($\Phi_{H2O2,\lambda}$). Thus, a knowledge gap needed to predict photochemical production of H_2O_2 in freshwaters is understanding how the chemical composition of terrestrially-derived DOM controls the magnitude of the $\Phi_{H2O2,\lambda}$.

The 5-fold range of the $\Phi_{H2O2,\lambda}$ observed in Lake Erie and one of its tributaries in this study is consistent with the few studies that, taken together, suggest a similarly large range in other freshwaters. Knowledge of the range in the magnitude of the $\Phi_{H2O2,\lambda}$ and confirmation of the expected exponential shape of the $\Phi_{H2O2,\lambda}$ spectrum in Lake Erie (Figure S11), allows a reassessment of photochemical sources of H_2O_2 in Lake Erie. Prior work concluded that photochemical production of H_2O_2 by CDOM rather than biological production of H_2O_2 by bacteria and phytoplankton could account for most of the H_2O_2 in Lake Erie only if the $\Phi_{H2O2,\lambda}$ was 3-fold higher than the literature-estimated $\Phi_{H2O2,\lambda}$ spectrum and if the slope of the $\Phi_{H2O2,\lambda}$ spectrum showed a less steep decrease with increasing wavelength than previously measured.[1]

Neither of those criteria were met in this study. The $\Phi_{H2O2,350}$ in this study was 1.3 - 2.3 fold higher in June and early July than the literature-estimated $\Phi_{H2O2,\lambda}$ spectrum used in Cory et al (2016), and the shape of the $\Phi_{H2O2,\lambda}$ spectrum was consistent with prior work.[16] Therefore, rates of photochemical production of H_2O_2 may be 1.3 - 2.3-fold higher nearshore in June and early July than previously estimated,[1] given the same range of CDOM concentrations and photon fluxes in this study. Thus, Cory et al. 2016 likely underestimated the contribution of photochemical production of H_2O_2 to the high H_2O_2 concentrations observed in Lake Erie in June and July prior to peak bloom toxicity.[1,8] Nonetheless, given that the magnitude of the $\Phi_{H2O2,350}$ in this study was not consistently 3-fold higher than used in prior work,[1] and considering that the photochemical production rates in this study were likely upper estimates applicable only for clear-sky days and low-turbidity waters, prior conclusions implicating biological production as an important source of H_2O_2 hold.[1] For example, Cory et al. previously reported a net biological production of H_2O_2 in Lake Erie of 1 mmol H_2O_2 m^{-2} d^{-1}. This rate was on the low end reported for eutrophic waters in Marsico et al. 2015,[14] likely because it was a net of biological production and decay of H_2O_2. Marsico et al. 2015 reported a maximum of 6 mmol m^{-2} d^{-1} for absolute rates of biological production of H_2O_2 (assuming 1 m depth) in eutrophic waters. Assuming 1 to 6 mmol m^{-2} d^{-1} is a representative range of biological production of H_2O_2 in Lake Erie, and using the range of 0.2 to 2.8 mmol H_2O_2 m^{-2} d^{-1} from photochemical H_2O_2 production in Lake Erie in this study (Figure 4), then photochemical production may account for ~ 20 - 30% of the total H_2O_2 production in the surface waters. However, there may be conditions when photochemical production dominates over biological production (e.g., the maximum photochemical production rate in this study is greater than the minimum rate of biological production reported in the literature). Thus, results from this study confirm that predicting H_2O_2 concentrations in freshwaters requires addressing the large knowledge gaps on the controls on

biological production and decay of H_2O_2

Acknowledgements: We thank NOAA-GLERL for access to Lake Erie water samples. McKenzie Powers, Colleen Yancey and Derek Smith assisted with sample collection. Dipesh Sedhai assisted with the data extraction from NCAR-TUV. This work was funded by NSF-OCE 1736629.

Conflict of Interest: There are no conflicts to declare.

Figure descriptions

Figure 1: The average experimental rate of H_2O_2 production ($P_{H2O2,exp}$) vs. CDOM concentration (a_{305}) in the Maumee River and Lake Erie. Error bars on $P_{H2O2,exp}$ show ± 1 SE of experimental replicates (n=3). The slopes of linear regressions of $P_{H2O2,exp}$ vs. a_{305} were not significantly different between WE2, high bloom biomass and WE4 ($p > 0.05$). Dashed line shows the linear regression fit for all Lake Erie waters i.e., WE2, high bloom biomass and WE4 ($R^2 = 0.76$; $p < 0.0001$).

Figure 2: Average apparent quantum yield for H_2O_2 production at 350 nm ($\Phi_{H2O2,350}$) in the Maumee River and Lake Erie corrected to 25 ºC. Error bars show ± 1 standard error (n = 4 for the Maumee River, n = 17 for WE2, n = 8 for high bloom biomass and n = 10 for WE4).

Figure 3: Photochemical production of H_2O_2 by CDOM over depth of 1 m at WE2 in Lake Erie in summer 2019. A) Daily total photon flux reaching the surface of Lake Erie ($E_{0,\lambda}$ modeled for 7am-7pm Eastern Standard Time). B) CDOM absorption coefficient at 305 nm (a_{305}). C) Apparent quantum yield for H_2O_2 production at 350 nm ($\Phi_{H2O2,350}$). D) Photochemical production rate of H_2O_2 at WE2 in Lake Erie ($P_{H2O2,lake}$). Error bars show ± 1 standard error of experimental replicates (n = 3).

Figure 4: Effect of CDOM, photon flux ($E_{0,\lambda}$) and apparent quantum yield spectrum ($\Phi H2O2,\lambda$) on photochemical production rates of H_2O_2 ($P_{H2O2,\ lake}$) at WE2 (A) and WE4 (B). For each scenario in A and B, $P_{H2O2,lake}$ was calculated as in *Eq.3* and *Eq.5*. By holding two variables constant at the average and one variable was varied using the maximum, average to minimum values observed respectively at WE2 and WE4 (Table S1).

Table 1: Water and DOC chemistry in the Maumee River and Lake Erie waters.

		Maumee River	**Lake Erie**			
			All Lake Erie	**WE2**	**High bloom biomass**	**WE4**
	n	**4**	**42**	**17**	**8**	**17**
	Units					
Water Temperature	(ºC)	25 ± 2	23 ± 1	23 ± 1	25 ± 1	22 ± 1
pH		8.9 ± 0.1	8.7 ± 0.1	8.8 ± 0.1	8.9 ± 0.2	8.6 ± 0.1
Specific conductivity	$\mu S\ cm^{-1}$	407 ± 44	283 ± 7	306 ± 11	315 ± 5	245 ± 7
DOC	µM C	656 ± 7	346 ± 20	408 ± 20	494 ± 17	216 ± 13
a_{305}	m^{-1}	27.2 ± 1.8	9.0 ± 1.0	12.0 ± 1.5	14.3 ± 1.5	3.6 ± 0.6
Spectral slope ratio (S_R)		0.86 ± 0.03	1.22 ± 0.07	1.06 ± 0.03	0.98 ± 0.07	1.49 ± 0.14
$SUVA_{254}$	$L\ mg\ C^{-1}m^{-1}$	2.97 ± 0.18	1.89 ± 0.09	2.22 ± 0.13	2.18 ± 0.12	1.43 ± 0.09
Fluorescence Index (FI)		1.57 ± 0.01	1.60 ± 0.01	1.58 ± 0.01	1.61 ± 0.01	1.61 ± 0.02
FDOM T/A		0.15 ± 0.02	0.33 ± 0.02	0.26 ± 0.02	0.24 ± 0.01	0.45 ± 0.04

All values are average ± 1 standard error

References

1 R. M. Cory, T. W. Davis, G. J. Dick, T. Johengen, V. J. Denef, M. A. Berry, S. E. Page, S. B. Watson, K. Yuhas and G. W. Kling, Seasonal dynamics in dissolved organic matter, hydrogen peroxide, and cyanobacterial blooms in Lake Erie, *Front Mar Sci*, 2016, **3**, 54.

2 C. M. Hansel and J. M. Diaz, Production of extracellular reactive oxygen species by marine biota, *Annu. Rev. Mar. Sci.* 2021, **13**, 177–200.

3 J. M. O'Neil, T. W. Davis, M. A. Burford and C. J. Gobler, The rise of harmful cyanobacteria blooms: The potential roles of eutrophication and climate change, *Harmful Algae*, 2012, **14**, 313–334.

4 F. L. Hellweger, R. M. Martin, F. Eigemann, D. J. Smith, G. J. Dick and S. W. Wilhelm, Models predict planned phosphorus load reduction will make Lake Erie more toxic, *Science,* 2022, **376**, 1001–1005.

5 W. J. Cooper and R. G. Zika, Photochemical formation of hydrogen peroxide in surface and ground waters exposed to sunlight, *Science*, 1983, **220**, 711–2.

6 N. Scully, D. McQueen, D. Lean and W. Cooper, Hydrogen peroxide formation: the interaction of ultraviolet radiation and rissolved organic carbon in lake waters along a 43-75∘ N gradient, *Limnol Oceanogr*, 2010, **41**, 540-548.

7 C. M. Febria, L. F. Lesack, J. al Gareis and M. L. Bothwell, Patterns of hydrogen peroxide among lakes of the Mackenzie Delta, western Canadian Arctic, *Canadian Journal of Fisheries and Aquatic Sciences*, 2006, **63**, 2107–2118.

8 R. M. Cory, T. W. Davis, G. J. Dick, T. Johengen, V. J. Denef, M. Berry, S. E. Page, S. B. Watson, K. Yuhas and G. W. Kling, Corrigendum: seasonal dynamics in dissolved organic matter, hydrogen peroxide, and cyanobacterial blooms in Lake Erie, *Front Mar Sci*, 2017, 4.

9 R. G. Petasne and R. G. Zika, *Nature*, 1987, 325, 516–518.

10 W. J. Cooper, R. G. Zika, R. G. Petasne and J. M. Plane, Photochemical formation of hydrogen peroxide in natural waters exposed to sunlight., *Environ Sci Technol*, 1988, **22**, 1156–60.

11 Y. Zhang, R. del Vecchio and N. v. Blough, Investigating the Mechanism of Hydrogen Peroxide Photoproduction by Humic Substances, *Environ Sci Technol*, 2012, **46**, 11836–11843.

12 A. W. Vermilyea, S. P. Hansard and B. M. Voelker, Dark production of hydrogen peroxide in the Gulf of Alaska, *Limnol Oceanogr*, 2010, **55**, 580–588.

13 T. C. Dixon, a W. Vermilyea, D. T. Scott and B. M. Voelker, Hydrogen peroxide dynamics in an agricultural headwater stream: Evidence for significant nonphotochemical production, *Limnol Oceanogr*, 2013, **58**, 2133–2144.

14 R. M. Marsico, R. J. Schneider, B. M. Voelker, T. Zhang, J. M. Diaz, C. M. Hansel and S. Ushijima, Spatial and temporal variability of widespread dark production and decay of hydrogen peroxide in freshwater, *Aquat Sci*, 2015, **77**, 523–533.

15 J. W. Moffett and O. C. Zafiriou, An investigation of hydrogen peroxide chemistry in surface waters of Vineyard Sound with H218O2 and 18O2, *Limnol Oceanogr*, 1990, **35**, 1221–1229.

16 D. J. Kieber, G. W. Miller, P. J. Neale and K. Mopper, Wavelength and temperature-dependent apparent quantum yields for photochemical formation of hydrogen peroxide in seawater, *Environ Sci Process Impacts*, 2014, **16**, 777–91.

17 L. C. Powers and W. L. Miller, Blending remote sensing data products to estimate photochemical production of hydrogen peroxide and superoxide in the surface ocean, *Environ Sci Process Impacts*, 2014, **16**, 792–806.

18 D. W. O'Sullivan, P. J. Neale, R. B. Coffin, T. J. Boyd and C. L. Osburn, Photochemical production of hydrogen peroxide and methylhydroperoxide in coastal waters, *Mar Chem*, 2005, **97**, 14–33.

19 D. T. Monteith, J. L. Stoddard, C. D. Evans, H. a de Wit, M. Forsius, T. Høgåsen, A. Wilander, B. L. Skjelkvåle, D. S. Jeffries, J. Vuorenmaa, B. Keller, J. Kopácek and J. Vesely, Dissolved organic carbon trends resulting from changes in atmospheric deposition chemistry, *Nature*, 2007, **450**, 537–540.

20 C. E. Williamson, E. P. Overholt, R. M. Pilla, T. H. Leach, J. A. Brentrup, L. B. Knoll, E. M. Mette and R. E. Moeller, Ecological consequences of long-term browning in lakes, *Sci Rep*, 2015, **5**, 18666.

21 H. A. de Wit, J. L. Stoddard, D. T. Monteith, J. E. Sample, K. Austnes, S. Couture, J. Fölster, S. N. Higgins, D. Houle, J. Hruška, P. Krám, J. Kopáček, A. M. Paterson, S. Valinia, H. van Dam, J. Vuorenmaa and C. D. Evans, Cleaner air reveals growing influence of climate on dissolved organic carbon trends in northern headwaters, *Environmental Research Letters*, 2021, **16**, 104009.

22 R. Wolf, J. E. Thrane, D. O. Hessen and T. Andersen, Modelling ROS formation in boreal lakes from interactions between dissolved organic matter and absorbed solar photon flux, *Water Res*, 2018, **132**, 331–339.

23 H. W. Paerl and T. G. Otten, Blooms bite the hand that feed them, *Science*, 2013, **342**, 433–434.

24 R. M. Cory, K. H. Harrold, B. T. Neilson and G. W. Kling, Controls on dissolved organic matter (DOM) degradation in a headwater stream: the influence of photochemical and hydrological conditions in determining light-limitation or substrate-limitation of photo-degradation, *Biogeosciences*, 2015, **12**, 6669–6685.

25 D. B. Bunnell, S. A. Ludsin, R. L. Knight, L. G. Rudstam, C. E. Williamson, T. O. Höök, P. D. Collingsworth, B. M. Lesht, R. P. Barbiero, A. E. Scofield, E. S. Rutherford, L. Gaynor, H. A. Vanderploeg and M. A. Koops, Consequences of changing water clarity on the fish and fisheries of the laurentian great lakes, *Canadian Journal of Fisheries and Aquatic Sciences*, 2021, **78**, 1524–1542.

26 A. M. Michalak, E. J. Anderson, D. Beletsky, S. Boland, N. S. Bosch, T. B. Bridgeman, J. D. Chaffin, K. Cho, R. Confesor, I. Daloglu, J. v. DePinto, M. A. Evans, G. L. Fahnenstiel, L. He, J. C. Ho, L. Jenkins, T. H. Johengen, K. C. Kuo, E. LaPorte, X. Liu, M. R. McWilliams, M. R. Moore, D. J. Posselt, R. P. Richards, D. Scavia, A. L. Steiner, E. Verhamme, D. M. Wright and M. A. Zagorski, Record-setting algal bloom in Lake Erie caused by agricultural and meteorological trends consistent with expected future conditions, *Proc Natl Acad Sci U S A*, 2013, **110**, 6448–6452.

27 M. A. Berry, T. W. Davis, R. M. Cory, M. B. Duhaime, T. H. Johengen, G. W. Kling, J. A. Marino, P. A. den Uyl, D. Gossiaux, G. J. Dick and V. J. Denef, Cyanobacterial harmful algal blooms are a biological disturbance to Western Lake Erie bacterial communities, *Environ Microbiol*, 2017, **19**, 1149-1162.

28 A. M. Culbertson, J. F. Martin, N. Aloysius and S. A. Ludsin, Anticipated impacts of climate change on 21st century Maumee River discharge and nutrient loads, *J Great Lakes Res*, 2016, **42**, 1332–1342.

29 K. Rowe, Mark; Kavanaugh, Experimental Lake Erie Harmful Algal Bloom (HAB) Tracker, https://www.glerl.noaa.gov/res/HABs_and_Hypoxia/habTracker.html, (accessed 25 July 2020).

30 G. W. Kling, G. W. Kipphut, M. M. Miller and W. JohN. O'Brien, Integration of lakes and streams in a landscape perspective: the importance of material processing on spatial patterns and temporal coherence, *Freshw Biol*, 2000, **43**, 477–497.

31 J. R. Helms, A. Stubbins, J. D. Ritchie, E. C. Minor, D. J. Kieber and K. Mopper, Absorption spectral slopes and slope ratios as indicators of molecular weight, source, and photobleaching of chromophoric dissolved organic matter, *Limnol Oceanogr*, 2008, **53**, 955–969.

32 J. L. Weishaar, G. R. Aiken, B. A. Bergamaschi, M. S. Fram, R. Fujii and K. Mopper, Evaluation of specific ultraviolet absorbance as an indicator of the chemical composition and reactivity of dissolved organic carbon, *Environ Sci Technol*, 2003, **37**, 4702–4708.

33 R. M. Cory, E. W. Boyer and D. M. McKnight, in *Forest hydrology and biogeochemistry: synthesis of past research and future directions*, ed. Levia, DF and Carlyle Moses, D and Tanaka, T, 2011, vol. 216, pp. 117–135.

34 J. O. Nriagu, G. Lawson, H. K. T. Wong and V. Cheam, Dissolved Trace Metals in Lakes Superior, Erie, and Ontario, *Environ Sci Technol*, 1996, **30**, 178–187.

35 J. C. Bowen, C. P. Ward, G. W. Kling and R. M. Cory, Arctic Amplification of Global Warming Strengthened by Sunlight Oxidation of Permafrost Carbon to CO_2, *Geophys Res Lett*, 2020, **47**, p.e2020GL087085.

36 S. S. Andrews, S. Caron and O. Zafiriou, Photochemical oxygen consumption in marine waters: a major sink for colored dissolved organic matter?, *Limnol. Oceanogr.*, 2000, **45**, 267–277.

37 C. P. Ward, J. C. Bowen, D. H. Freeman and C. M. Sharpless, Rapid and reproducible characterization of the wavelength dependence of aquatic photochemical reactions using light-emitting diodes, *Environ Sci Technol Lett*, 2021, **8**, 437–442.

38 D. W. King, W. J. Cooper, S. A. Rusak, B. M. Peake, J. J. Kiddle, D. W. O'Sullivan, M. L. Melamed, C. R. Morgan and S. M. Theberge, Flow injection analysis of H2O2 in natural waters using acridinium ester chemiluminescence: Method development and optimization using a kinetic model, *Anal Chem*, 2007, **79**, 4169–4176.

39 Y. Zhang, R. del Vecchio and N. v Blough, Investigating the mechanism of hydrogen peroxide photoproduction by humic substances, *Environ Sci Technol*, 2012, **46**, 11836-11843.

40 Quick TUV calculator, https://www.acom.ucar.edu/Models/TUV/Interactive_TUV/, (accessed 1 May 2020).

41 B. Wu, T. Liu, Y. Wang, G. Zhao, B. Chen and C. Chu, High sample throughput led reactor for facile characterization of the quantum yield spectrum of photochemically produced reactive intermediates, *Environ Sci Technol*, 2021, **55**, 16204–16214.

42 A. Marchisio, M. Minella, V. Maurino, C. Minero and D. Vione, Photogeneration of reactive transient species upon irradiation of natural water samples: Formation quantum yields in different spectral intervals, and implications for the photochemistry of surface waters, *Water Res*, 2015, **73**, 145–156.

43 C. A. Stow, Y. Cha, L. T. Johnson, R. Confesor and R. P. Richards, Long-Term and Seasonal Trend Decomposition of Maumee River Nutrient Inputs to Western Lake Erie, *Environ Sci Technol*, 2015, **49**, 3392-3400.

44 R. M. Cory, K. McNeill, J. P. Cotner, A. Amado, J. M. Purcell and A. G. Marshall, Singlet oxygen in the coupled photochemical and biochemical oxidation of dissolved organic matter, *Environ Sci Technol*, 2010, **44,** 3683-3689.

45 P. E. García, C. Queimaliños and M. C. Diéguez, Natural levels and photo-production rates of hydrogen peroxide (H2O2) in Andean Patagonian aquatic systems: Influence of the dissolved organic matter pool, *Chemosphere*, 2019, **217**, 550–557.

46 L. M. Mayer, L. L. Schick, K. R. Hardy and M. L. Estapa, Photodissolution and other photochemical changes upon irradiation of algal detritus, *Limnol Oceanogr*, 2009, **54**, 1688–1698.

47 C. M. Godwin, J. R. Zehnpfennig and D. R. Learman, Biotic and Abiotic Mechanisms of Manganese (II) Oxidation in Lake Erie, Frontiers in Environmental Science, 2020, **8**, 57.

48 National Centers for Environmental Information, https://www.ncei.noaa.gov/archive/archive-management-

system/OAS/bin/prd/jquery/accession/details/187718 (accessed 5 September 2022).

49 F. L. Hellweger, R. M. Martin, F. Eigemann, D. J. Smith, G. J. Dick and S. W. Wilhelm, Models predict planned phosphorus load reduction will make Lake Erie more toxic, *Science*, 2022, **376**, 1001–1005.

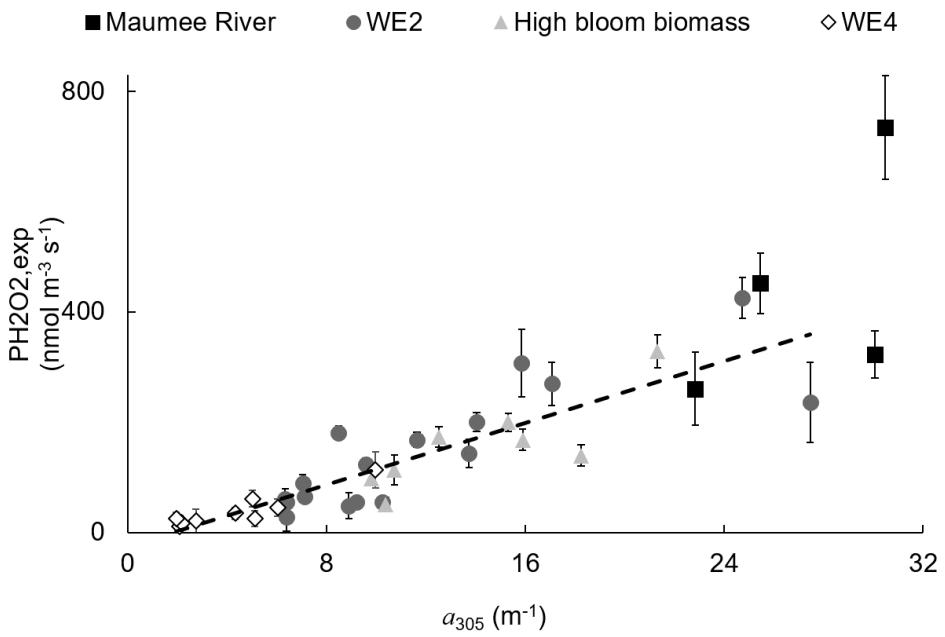

Figure 1: The average experimental rate of H_2O_2 production ($PH2O2_{,exp}$) vs. CDOM concentration (a_{305}) in the Maumee River and Lake Erie. Error bars on $PH2O2_{,exp}$ show ± 1 SE of experimental replicates (n=3). The slopes of linear regressions of $PH2O2_{,exp}$ vs. a_{305} were not significantly different between WE2, high bloom biomass and WE4 ($p > 0.05$). Dashed line shows the linear regression fit for all Lake Erie waters i.e., WE2, high bloom biomass and WE4 ($R2 = 0.76$; $p < 0.0001$).

548x361mm (59 x 59 DPI)

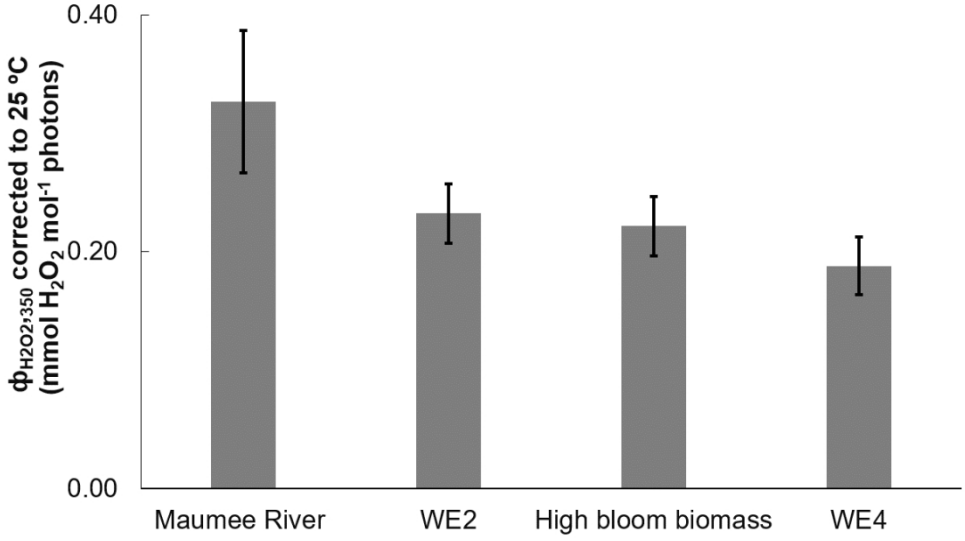

Figure 2: Average apparent quantum yield for H_2O_2 production at 350 nm ($\Phi_{H2O2,350}$) in the Maumee River and Lake Erie corrected to 25 °C. Error bars show ±1 standard error (n = 4 for the Maumee River, n = 17 for WE2, n = 8 for high bloom biomass and n = 10 for WE4).

545x335mm (59 x 59 DPI)

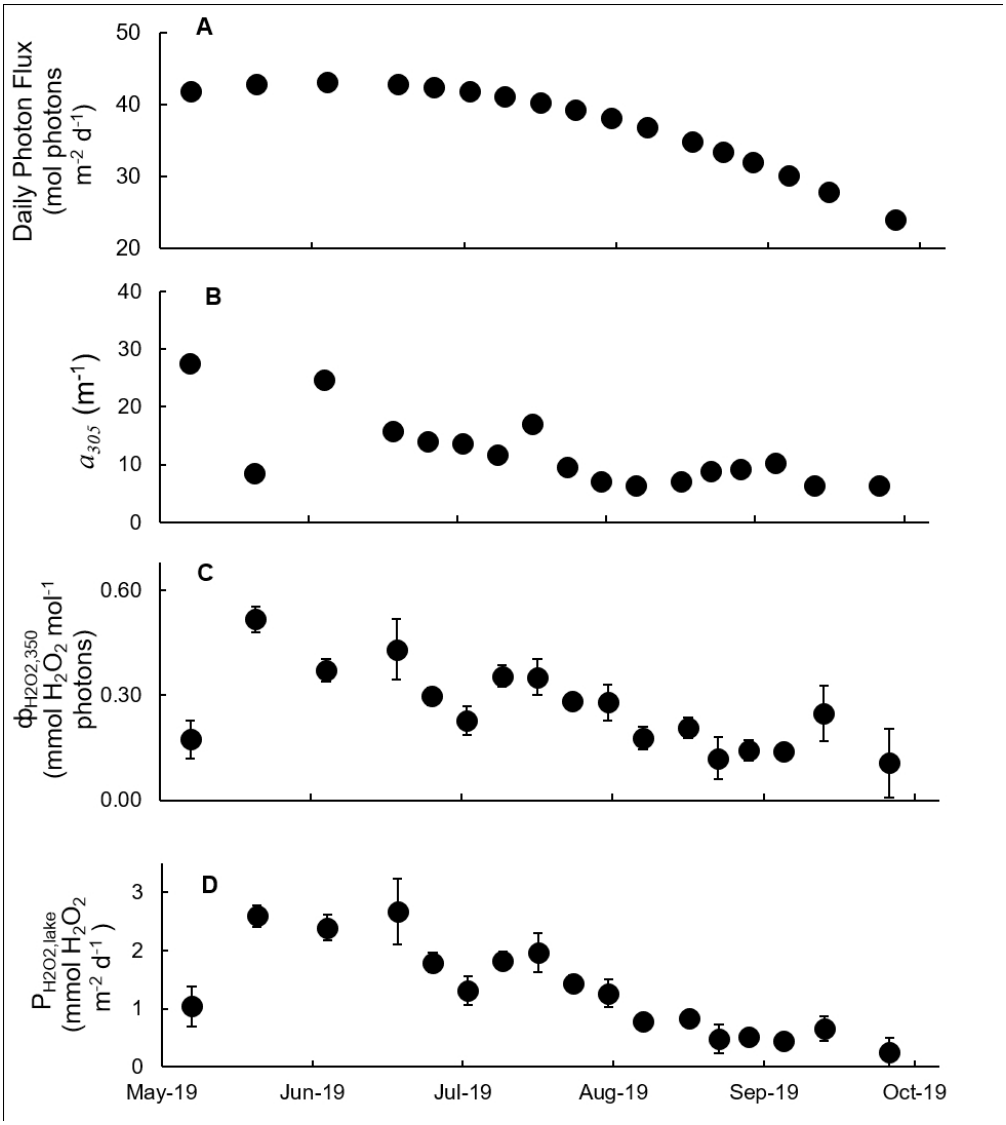

Figure 3: Photochemical production of H_2O_2 by CDOM over depth of 1 m at WE2 in Lake Erie in summer 2019. A) Daily total photon flux reaching the surface of Lake Erie ($E_{0,\lambda}$ modeled for 7am-7pm Eastern Standard Time). B) CDOM absorption coefficient at 305 nm (a_{305}). C) Apparent quantum yield for H_2O_2 production at 350 nm ($\Phi_{H2O2,350}$). D) Photochemical production rate of H_2O_2 at WE2 in Lake Erie ($PH2O2_{,lake}$). Error bars show ± 1 standard error of experimental replicates (n = 3).

419x468mm (59 x 59 DPI)

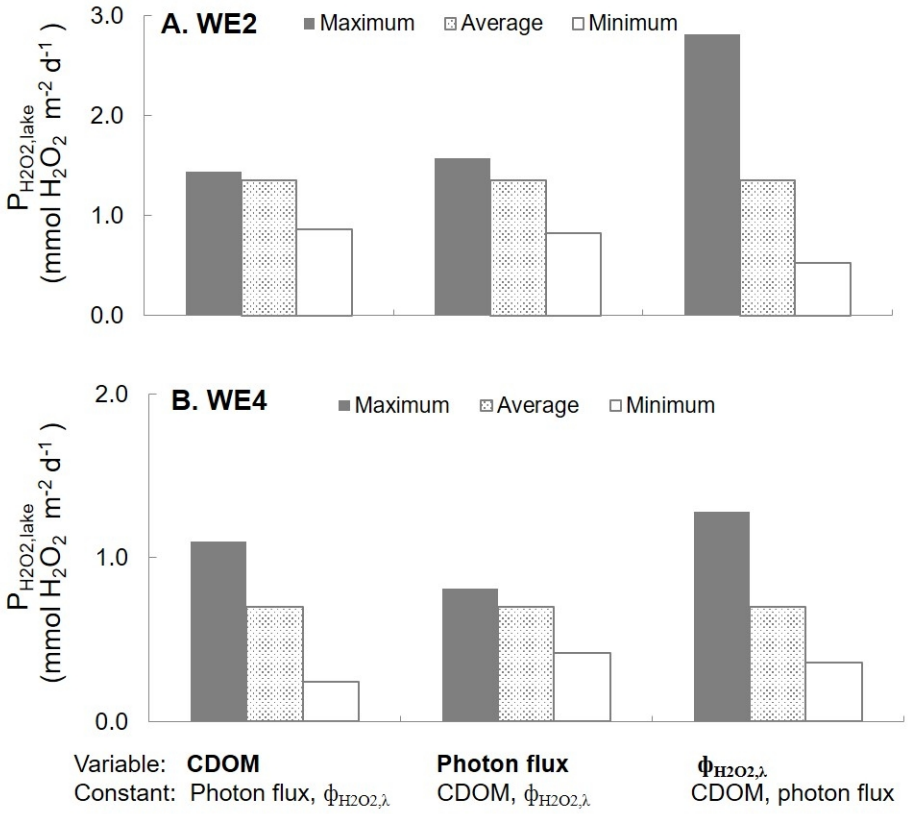

Figure 4: Effect of CDOM, photon flux ($E_{0,\lambda}$) and apparent quantum yield spectrum ($\Phi_{H2O2,\lambda}$) on photochemical production rates of H_2O_2 ($PH2O2_{,lake}$) at WE2 (A) and WE4 (B). For each scenario in A and B, $PH2O2_{,lake}$ was calculated as in Eq.3 and Eq.5. By holding two variables constant at the average and one variable was varied using the maximum, average to minimum values observed respectively at WE2 and WE4 (Table S1).

176x150mm (150 x 150 DPI)